Spline analysis of Holocene sediment magnetic records: Uncertainty estimates for field modeling

S. Panovska,[1] C. C. Finlay,[1] F. Donadini,[1] and A. M. Hirt[1]

Received 25 August 2011; revised 8 December 2011; accepted 12 December 2011; published 8 February 2012.

[1] Sediment and archeomagnetic data spanning the Holocene enable us to reconstruct the evolution of the geomagnetic field on time scales of centuries to millennia. In global field modeling the reliability of data is taken into account by weighting according to uncertainty estimates. Uncertainties in sediment magnetic records arise from (1) imperfections in the paleomagnetic recording processes, (2) coring and (sub) sampling methods, (3) adopted averaging procedures, and (4) uncertainties in the age-depth models. We take a step toward improved uncertainty estimates by performing a comprehensive statistical analysis of the available global database of Holocene magnetic records. Smoothing spline models that capture the robust aspects of individual records are derived. This involves a cross-validation approach, based on an absolute deviation measure of misfit, to determine the smoothing parameter for each spline model, together with the use of a minimum smoothing time derived from the sedimentation rate and assumed lock-in depth. Departures from the spline models provide information concerning the random variability in each record. Temporal resolution analysis reveals that 50% of the records have smoothing times between 80 and 250 years. We also perform comparisons among the sediment magnetic records and archeomagnetic data, as well as with predictions from the global historical and archeomagnetic field models. Combining these approaches, we arrive at individual uncertainty estimates for each sediment record. These range from 2.5° to 11.2° (median: 5.9°; interquartile range: 5.4° to 7.2°) for inclination, 4.1° to 46.9° (median: 13.4°; interquartile range: 11.4° to 18.9°) for relative declination, and 0.59 to 1.32 (median: 0.93; interquartile range: 0.86 to 1.01) for standardized relative paleointensity. These values suggest that uncertainties may have been underestimated in previous studies. No compelling evidence for systematic inclination shallowing is obtained from the analysis of the available database of Holocene sediment magnetic records. The analysis highlights the importance of collecting oriented cores, publishing and archiving unprocessed raw paleosecular variation determinations, and presenting a detailed chronology so that changes in the sedimentation rate can be assessed. With regard to future field models, workers should consider rejection of anomalous cores through comparisons to other sources and ensure that realistically large uncertainties are allocated to high-latitude declination records.

Citation: Panovska, S., C. C. Finlay, F. Donadini, and A. M. Hirt (2012), Spline analysis of Holocene sediment magnetic records: Uncertainty estimates for field modeling, *J. Geophys. Res.*, *117*, B02101, doi:doi:10.1029/2011JB008813.

1. Introduction

[2] The Earth's magnetic field is characterized by both its spatial morphology and temporal variation. Fluctuations with time scales of years to millennia are referred to as geomagnetic secular variation. The study of temporal variation with periods of hundreds to thousands of years requires very long records. Lake sediment magnetic records are important archives of geomagnetic field behavior on these time scales, particularly in the Holocene for which a large number of records exist compared to earlier times. The recorded signal exhibits variations, some of which are field behavior, but others are due to the effect of depositional and environmental changes. Their fidelity is subject to numerous interdependent factors, and it is probably not possible to completely isolate true variation of the Earth's magnetic field from that due to other sources. The major advantage of lake sediment records is that they are continuous in time and have a broad geographic distribution. In recent years there have been a number of corings conducted on new lake systems that have enhanced the global coverage.

[3] Geomagnetic field models, constructed either from modern [*Finlay et al.*, 2010], historical [*Jackson et al.*, 2000] or archeomagnetic and paleomagnetic data [*Korte and Constable*, 2003, 2005, 2011; *Korte et al.*, 2009, 2011; *Nilsson et al.*, 2010; *Pavón-Carrasco et al.*, 2010], provide a global picture of the geomagnetic field and its evolution both

[1]Institute of Geophysics, ETH Zürich, Zurich, Switzerland.

0148-0227/12/2011JB008813

at the Earth's surface and at the core mantle boundary. When field models are constructed, the reliability of underlying data is taken into consideration by weighting the data according to uncertainty estimates. Therefore, a pertinent question for attempts to accurately recover geomagnetic field behavior on time scales of centuries to millennia, is how to assign appropriate and consistent estimates of data uncertainty for lake sediment records.

[4] Uncertainties in archeomagnetic and paleomagnetic records are much higher than in direct field measurements. Many factors can influence the accuracy of these records, and unfortunately there is no simple theory of how uncertainties should be assigned. Previously, the uncertainties in declination and inclination have been estimated in a variety of ways. For example, records have been compared with the historical field model *gufm*1 [*Jackson et al.*, 2000] in overlapping time intervals [*Constable et al.*, 2000], or by assigning minimum uncertainties for different classes of data. Errors in the ages of paleomagnetic samples are another important source of uncertainty. In most cases, the age uncertainties range from a few decades to a few centuries, depending on the dating method. Radiocarbon (^{14}C) dating is commonly used, but some sediments are varved and ages can then be determined with close to annual accuracy, although there are also uncertainties associated with these methods [*Stanton et al.*, 2010; *Oldfield et al.*, 1997; *Stuiver and Reimer*, 1993; *Stuiver et al.*, 1998]. Ideally, all these sources of uncertainty should be taken into account during the modeling procedure.

[5] When quantifying uncertainties in sediment magnetic records, the process by which the sediments become magnetized must be considered. Sediments acquire the magnetization in a process known as depositional or detrital remanent magnetization (DRM) [*Johnson et al.*, 1948; *King*, 1955], which involves magnetic grains aligning with the ambient magnetic field in the water column. The original DRM is often destroyed by sediment compaction and diagenesis, and the remanent magnetization that eventually locks in is then refereed to as postdepositional remanent magnetization (pDRM) [*Irving and Major*, 1964]. Inclination flattening is proposed to be another effect in the lake sediment records due to the compaction of the sediments [cf. *Tauxe*, 2005; *Tauxe et al.*, 2008]. The acquisition process occurs over a certain time period and often leads to a smoothed record of the actual field behavior. The amount of smoothing depends on factors including sample size, porosity, sedimentation rate, grain size, bioturbation and the lock-in depth. Bioturbation occurs in the surface mixed layer that has an estimated mean value of 9.8 cm for marine sediments [*Boudreau*, 1994, 1998], which causes a time lag between the sediment deposition and magnetization ages. The ambient magnetic field vector only starts to lock below the mixed layer when the sediment becomes consolidated. Estimates of the lock-in depth vary over a range of values on the order of 10–20 cm in the deep sea sediments [*Hyodo*, 1984; *Yamazaki*, 1984; *Lund and Keigwin*, 1994; *Channell and Guyodo*, 2004; *Suganuma et al.*, 2011]. An average lock-in depth of 24 cm, corresponding to 150 years, has been determined in the sediments from three maar lakes from the West Eifel (Germany) by *Stockhausen* [1998] from comparison of stacked sediment data with archeomagnetic data. *Roberts and Winklhofer* [2004] have produced models of the lock-in process that display a lock-in depth of 10 cm (below the surface mixed layer), with 95% of the pDRM being locked in within the first 5 cm. This depth is important because together with the sedimentation rate it provides an estimate of the minimum smoothing time expected due to the sediment magnetization process.

[6] In this paper we focus on deriving uncertainty estimates for Holocene sediment magnetic records via statistical modeling and comparisons with other sources. Our approach is designed to account for the diversity among the records, for example, the measurement procedures, paleomagnetic component determination, or dating techniques. Smoothing spline models are used to investigate the random variability present in each record. The degree of smoothing is determined using the technique of cross validation [*Green and Silverman*, 1994], but a lower limit of smoothing is also defined based on an assumed lock-in depth and the mean sedimentation rate for each record. Variance is estimated from the scatter of the data about the spline model. Further tests to evaluate the accuracy of the lake sediment records are performed by comparing each record to neighboring lake sediment records, and archeomagnetic data within a 5° area of latitude and longitude. Finally, we also investigate the differences between the sediment records and the predictions of global field models *gufm*1 and ARCH3k.1 [*Korte et al.*, 2009], but only where nearby archeomagnetic data exist. This allows us to investigate any systematic uncertainties that may be present in the records. We also discuss the implications of our findings, and perspectives for future sediment studies, as well as for the next generation of Holocene field models.

2. Holocene Sediment Magnetic Records

[7] In this study we used the database compiled by *Korte et al.* [2005], updated by *Donadini et al.* [2009], and expanded with new records from 13 additional locations [*Korte et al.*, 2011]. Most of the records come from lakes (90%), the remainder are marine sediment records from a limited catchment basin. Table 1 lists the codes of name, location, mean sedimentation rate and references to the individual sediment records. The Finnish lake records (FIN) contains multiple lake sediment cores, with the Lake Lehmilampi and Lake Kortejärvi stacked and smoothed together [*Haltia-Hovi et al.*, 2010]. Three marine sediment records from the Ionian Sea, Adriatic Sea (core AD2) and Tyrrhenian Sea were excluded from the analysis due to either their very low sedimentation rate (approximately 0.1 mm/yr), or questions concerning disturbances in the Tyrrhenian cores due to their high water content [*Vigliotti*, 2006]. A further two records from Byestadsjön, Sweden [*Snowball and Sandgren*, 2004; *Snowball et al.*, 2007] and the Larsen Ice Shelf, Antarctic Peninsula [*Brachfeld et al.*, 2003] were also omitted, because their ages were determined by a paleomagnetic method rather than by independent dating. The spatial and temporal distributions of the geomagnetic field elements declination (D), inclination (I), and relative paleointensity (RPI) from this data set are illustrated in Figure 1. The southern hemisphere is poorly represented for both directional and intensity data, while there is a high

Table 1. Summary of Uncertainty Estimates and Smoothing Times for Holocene Sediment Records[a]

			σ_{rss}[c]			σ_c[d]			σ_I[e]			T_{ss}[f] (years)			
Code	Location	SR[b] (mm/yr)	D (deg)	I (deg)	RPI	D (deg)	I (deg)	RPI	D (deg)	I (deg)	RPI	D	I	RPI	Ref.[g]
AAM	Alaskan Margin, Arctic Sea	1.93	27.8	2.2	0.43			29.9	5.7	0.81	52.2	52.0	52.0		1
AD1	Adriatic Sea, Italy	0.54	-	1.6	0.24	-	8.1		-	7.4	0.84	-	185.4	186.9	2
ANN	Lac d'Annecy, France	1.8	9.7	3.6	-	21.7	8.0	-	21.5	9.1	-	56.8	84.6	-	3
ARA	Lake Aral, Kazakhstan	10.2	1.6	0.5	-			-	11.0	5.3	-	34.0	37.4	-	4
ASL	Lake Aslikul, Russia	0.75	1.3	0.6	-			-	11.0	5.3	-	134.1	133.4	-	5
BAI	Lake Baikal, Russia	0.14	10.3	3.5	0.53			1.32	15.0	6.3	1.27	719.4	717.9	717.6	6
BAM	Lake Barombi Mbo, Cameroun	1.8	1.7	1.5	-			-	11.1	5.6	-	79.7	84.3	-	7
BAR	Lake Barrine, Australia	0.75	20.4	9.5	1.05				23.1	10.9	1.32	134.1	134.8	136.6	8, 9
BEA	Beaufort Sea, Arctic Ocean	1.35	22.2	2.3	0.22				24.8	5.9	0.84	76.0	74.1	74.9	10
BEG	Lake Begoritis, Greece	1.0	5.4	2.3	-	10.0	3.7	-	9.4	2.5	-	101.9	100.3	-	11
BI2	Lake Biwa 2, Japan	0.4	1.8	1.2	0.61				11.1	5.5	1.01	252.0	252.9	251.0	12
BIR	Birkat Ram, Israel	1.6	7.3	5.1	0.34			1.34	13.1	7.4	1.30	64.4	66.4	68.9	13, 14
BIW	Lake Biwa, Japan	1.21	1.2	0.7	-	5.2	5.0	-	4.1	3.5	-	82.9	83.0	-	15
BLM	Lake Bullenmerri, Australia	0.88	4.9	3.3	-			-	12.0	6.3	-	179.5	186.7	-	16
BOU	Lac du Bourget, France	3.75	8.2	2.8	-	14.6	3.2	-	14.3	2.9	-	36.5	93.6	-	3
CAM	Brazo Campanario, Argentina	0.77	5.3	2.1	-			-	12.2	5.8	-	130.4	130.7	-	17
CHU	Chukchi Sea, Arctic Ocean	1.3	14.0	2.3	0.18				17.7	5.9	0.83	78.5	78.6	77.0	10
DES	Dead Sea, Israel	2.0	12.5	7.0	-			-	16.6	8.8	-	50.2	50.2	-	18
EAC	Lake Eacham, Australia	1.1	27.4	8.9	0.99				29.5	10.4	1.28	91.1	100.7	91.4	8, 9
EIF	Eifel maars, Germany	1.02	4.3	1.8	-	8.7	5.4	-	8.3	4.3	-	126.0	113.9	-	19
ERH	Erhai Lake, China	0.9	9.0	7.8	-			-	14.2	9.4	-	111.2	132.8	-	20
ERL	Erlongwan Lake, China	0.27	5.8	3.1	-			-	12.4	6.2	-	370.6	377.0	-	21
ESC	Lake Escondido, Argentina	0.3	11.5	2.9	0.62				15.8	6.1	1.02	335.0	333.6	333.7	22, 23
FAN	Lake Fangshan, China	0.5	6.5	9.8	-			-	12.7	11.2	-	201.5	201.2	-	24
FIN	Finnish Lakes, Finland	0.64	2.7	0.9	-			-	11.3	5.5	-	158.0	158.2	-	25
FIS	Fish Lake, USA	0.8	5.0	3.3	-			-	12.0	6.3	-	125.8	125.2	-	26
FRG	Frängsjön, Sweden	0.4	9.2	2.4	0.49				14.3	5.9	0.94	255.7	253.5	254.1	27, 28
FUR	Furskogstjärnet, Sweden	0.41	10.5	2.6	0.22				15.2	6.0	0.83	250.7	244.7	245.8	27, 29
GAR	Gardar Drift, North Atlantic	0.3	17.4	3.3	0.32				20.5	6.3	0.87	341.7	333.6	334.7	30
GEI	Llyn Geirionydd, UK	0.31	3.5	1.4	-	9.2	5.7	-	8.8	5.2	-	328.0	323.1	-	31
GHI	Cape Ghir, NW Afr. Margin	0.6	9.2	4.7	0.56				14.3	7.2	0.98	229.2	167.1	167.0	32
GNO	Lake Gnotuk, Australia	0.39	6.9	5.2	-			-	12.9	7.5	-	257.9	257.1	-	16
GRE	Greenland, North Atlantic	1.0	16.9	2.1	-			-	20.1	5.8	-	102.8	102.5	-	33
HUR	Lake Huron, USA	0.63	26.3	5.7	-			-	28.5	7.9	-	159.1	164.5	-	34
ICE	Iceland, North Atlantic	2.0	18.3	3.0	-			-	21.3	6.1	-	50.1	50.1	-	33
KEI	Lake Keilambete, Australia	0.31	7.9	3.6	-			-	13.5	6.5	-	326.0	329.3	-	16
KYL	Kylen Lake, Minnesota	0.8	7.0	2.0	-			-	12.9	5.8	-	125.1	125.6	-	35
LAM	Lake Lama, Russia	0.59	30.7	5.3	-			-	32.6	7.6	-	170.1	173.5	-	36
LEB	Lake LeBoeuf, USA	2.1	3.8	1.0	0.47				11.6	5.5	0.93	163.1	170.3	52.2	37
LOM	Loch Lomond, UK	0.31	3.4	1.5	-	9.6	3.2	-	9.3	3.2	-	325.7	322.6	-	38
LOU	Louis Lake, USA	0.2	45.6	5.4	-			-	46.9	7.6	-	503.0	980.0	-	39
LSC	Lake St.Croix, USA	2.5	5.2	2.7	0.29				12.1	6.0	0.86	77.4	79.7	54.8	35
MAR	Mara Lake, Canada	1.22	1.7	0.7	-			-	11.1	5.4	-	82.0	82.1	-	40
MEE	Meerfelder Maar, Germany	1.0	27.2	11.6	-	24.6	6.7	-	24.5	6.1	-	100.0	102.9	-	41
MEZ	Lago di Mezzano, Italy	0.9	6.4	3.0	0.63	21.8	6.8	0.65	21.6	7.4	0.59	111.5	114.6	111.8	42
MNT	Lago Morenito, Argentina	0.3	6.4	3.5	-			-	12.7	6.4	-	334.3	335.9	-	17
MOR	Lac Morat, Switzerland	0.9	9.9	2.1	-	6.2	5.6	-	5.4	4.4	-	113.5	112.1	-	3
MOT	Mötterudstjärnet, Sweden	0.41	10.9	4.0	0.47				15.4	6.7	0.93	245.8	254.9	247.1	27, 29
NAR	Lake Naroch, Belorussia	0.64	2.2	0.8	-			-	11.2	5.4	-	156.9	156.7	-	43
NAU	Nautajärvi, Finland	0.6	5.6	1.8	0.50		6.7		12.3	8.2	0.95	167.1	174.4	167.2	27, 44
NEM	Lake Nemi, Italy	1.1	4.4	2.6	-	23.3	8.1	-	23.2	9.8	-	91.4	92.8	-	2
PAD	Palmer Deep, Antarctic Pen.	2.5	33.4	4.4	0.30				35.1	7.0	0.86	40.3	40.1	40.3	45
PEP	Lake Pepin, USA	1.5	-	2.9	0.33	-			-	6.1	0.87	-	66.8	68.0	46
POH	Pohjajärvi, Finland	1.04	6.4	2.5	0.46				12.7	5.9	0.93	103.1	96.6	96.4	47
POU	Lake Pounui, New Zealand	0.96	2.2	1.2	-			-	11.2	5.5	-	111.0	127.2	-	48
SAG	Saguenay Fjord, Canada	1.5	5.8	2.2	-			-	12.4	5.8	-	67.0	67.1	-	49
SAN	Hoya de San Nicolas, Mexico	0.38	12.2	9.9	-			-	16.4	11.3	-	268.7	264.7	-	50
SAR	Sarsjön, Sweden	0.4	34.9	2.1	0.38				36.6	5.8	0.89	252.9	250.4	250.6	27, 28
SAV	Savijärvi, Finland	0.42	11.8	2.1	-			-	16.1	5.8	-	238.7	242.1	-	27, 51
SCL	Lake Shuangchiling, China	2.2	7.8	5.4	-			-	13.4	7.7	-	45.5	45.6	-	52
STL	St. Lawrence Est., Canada	1.5	5.3	1.9	0.29				12.2	5.7	0.86	67.3	67.4	67.5	53
SUP	Lake Superior, USA	1.08	14.3	1.9	-			-	18.0	5.7	-	93.4	93.3	-	54
TRE	Laguna El Trébol, Argentina	0.4	5.9	1.6	0.50				12.4	5.6	0.95	252.3	252.3	252.1	55, 56
TRI	Lake Trikhonis, Greece	1.0	5.4	4.4	-	7.6	5.2	-	6.8	3.3	-	100.2	100.7	-	11
TUR	Lake Turkana, Kenya	1.9	-	7.6	-	-		-	-	9.3	-	-	59.7	-	57
VAT	Vatndalsvatn, Iceland	0.78	16.6	3.4	-			-	19.9	6.4	-	129.9	129.3	-	58
VIC	Lake Victoria, Uganda	1.0	7.7	4.5	-			-	13.3	7.0	-	100.5	103.8	-	59
VOL	Lake Volvi, Greece	2.5	13.8	6.7	-	14.6	5.8	-	14.3	4.0	-	40.6	40.6	-	11

Table 1. (continued)

Code	Location	SR[b] (mm/yr)	σ_{rss}[c] D (deg)	σ_{rss}[c] I (deg)	σ_{rss}[c] RPI	σ_c[d] D (deg)	σ_c[d] I (deg)	σ_c[d] RPI	σ_l[e] D (deg)	σ_l[e] I (deg)	σ_l[e] RPI	T_{ss}[f] (years) D	T_{ss}[f] (years) I	T_{ss}[f] (years) RPI	Ref.[g]
VUK	Vukonjärvi, Finland	0.5	10.7	3.4	-			-	15.3	6.4	-	200.4	201.1	-	60
WAI	Lake Waiau, Hawaii	0.4	5.3	3.1	-	8.1	6.1	-	6.5	6.2	-	250.6	251.1	-	61
WAS	West Amundsen Sea	0.2	-	-	1.00	-	-		-	-	1.29	-	-	803.2	62
WIN	Lake Windermere, UK	0.5	1.6	0.5	-	6.4	5.0	-	5.8	2.5	-	204.2	202.1	-	31
WPA	West Pacific	3.9	-	1.7	0.15	-			-	5.6	0.82	-	27.0	28.9	63

[a]Dash stands for the absence of a particular component.
[b]SR refers to the mean sedimentation rate in mm/yr.
[c]σ_{rss} refers to the random uncertainty component obtained from the robust smoothing spline fit.
[d]σ_c is an uncertainty from the comparison with archeomagnetic estimates. Empty space in the columns for σ_c means no comparison is possible.
[e]σ_l is the overall estimated uncertainty for the sediment records.
[f]T_{ss} is the smoothing time obtained from the robust smoothing spline analysis.
[g]References: 1, *Lisé-Pronovost et al.* [2009]; 2, *Vigliotti* [2006]; 3, *Hogg* [1978]; 4, *Nourgaliev et al.* [2003]; 5, *Nourgaliev et al.* [1996]; 6, *Peck et al.* [1996]; 7, *Thouveny and Williamson* [1988]; 8, *Constable and McElhinny* [1985]; 9, *Constable* [1985]; 10, *Barletta et al.* [2008]; 11, *Creer et al.* [1981]; 12, *Hayashida et al.* [2007]; 13, *Frank et al.* [2002b]; 14, *Frank et al.* [2003]; 15, *Ali et al.* [1999]; 16, *Barton and McElhinny* [1981]; 17, *Creer et al.* [1983]; 18, *Frank et al.* [2007]; 19, *Stockhausen* [1998]; 20, *Hyodo et al.* [1999]; 21, *Frank* [2007]; 22, *Gogorza et al.* [2002]; 23, *Gogorza et al.* [2004]; 24, *Zhu et al.* [1994]; 25, *Haltia-Hovi et al.* [2010]; 26, *Verosub et al.* [1986]; 27, *Snowball et al.* [2007]; 28, *Snowball and Sandgren* [2002]; 29, *Zillén* [2003]; 30, *Channell et al.* [1997]; 31, *Turner and Thompson* [1981]; 32, *Bleil and Dillon* [2008]; 33, *Stoner et al.* [2007]; 34, *Mothersill* [1981]; 35, *Lund and Banerjee* [1985]; 36, *Frank et al.* [2002a]; 37, *King* [1983]; 38, *Turner and Thompson* [1979]; 39, *Geiss et al.* [2007]; 40, *Turner* [1987]; 41, *Brown* [1991]; 42, *Brandt et al.* [1999]; 43, *Nourgaliev et al.* [2005]; 44, *Ojala and Saarinen* [2002]; 45, *Brachfeld et al.* [2000]; 46, *Brachfeld and Banerjee* [2000]; 47, *Saarinen* [1998]; 48, *Turner and Lillis* [1994]; 49, *St-Onge et al.* [2004]; 50, *Chaparro et al.* [2008]; 51, *Ojala and Tiljander* [2003]; 52, *Yang et al.* [2009]; 53, *St-Onge et al.* [2003]; 54, *Mothersill* [1979]; 55, *Irurzun et al.* [2006]; 56, *Gogorza et al.* [2006]; 57, *Barton and Torgersen* [1988]; 58, *Thompson and Turner* [1985]; 59, *Mothersill* [1996]; 60, *Huttunen and Stober* [1980]; 61, *Peng and King* [1992]; 62, *Hillenbrand et al.* [2010]; and 63, *Richter et al.* [2006].

concentration of observations in the European region. Histograms of the temporal distribution show that the number of data records increases toward more recent times, and that intensity data constitute a rather small fraction of the total data set. The length of the records range from 1150 to 11,855 years, taking into consideration only the data from the Holocene.

[8] Radiocarbon (^{14}C) dating is the method that is most commonly used; it is only possible when organic material is present in the sediments. Some sediments, in particular the Fennoscandinavian records [*Snowball et al.*, 2007], are varved and can be dated by varve counting, which gives more precise age scales and smaller age uncertainties. Almost half of the radiocarbon dated records have independent dating points (tephra, varves or pollen) to improve their age-depth model.

[9] To obtain directional and relative paleointensity data, a range of different sampling strategies, tests and normalization techniques have been used. Only 12% of the results in the whole database were acquired by U channel measurements; most studies involved discrete samples allowing higher temporal resolution. Directional information from the majority of the records has been recovered by selecting pilot samples from different lithological sections and conducting stepwise alternating field (AF) demagnetization to establish the characteristic remanent magnetization.

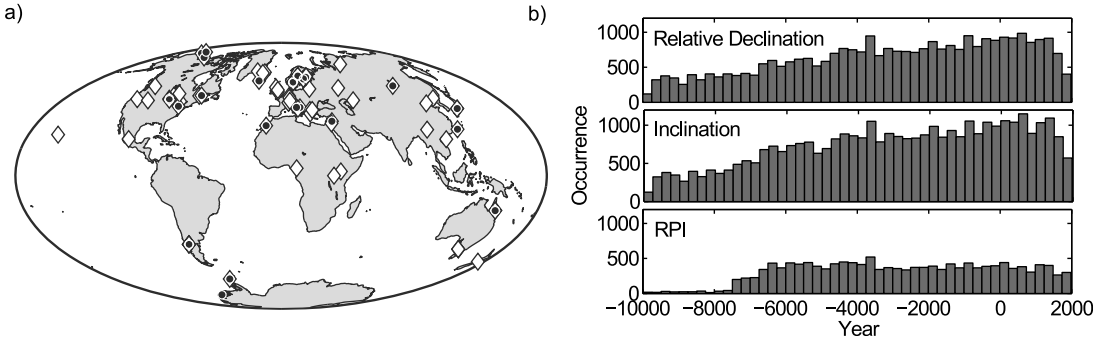

Figure 1. (a) The global spatial distribution of Holocene sediment records used in this study, directional (declination or inclination) data (white diamonds), and relative paleointensity (black circles). Only inclination data are available for the records AD1, PEP, TUR, and WPA. (b) Temporal distribution of declination, inclination, and relative paleointensity during the Holocene period. The time scale is in units of years (AD/BC), following the convention used in the field modeling community. Data are grouped in 250 year bins.

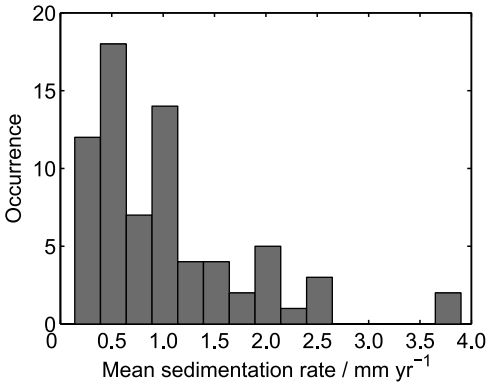

Figure 2. Histogram of the mean sedimentation rate in the Holocene sediment records in this study (Table 1). The mean sedimentation rate of Lake Aral is omitted from this histogram due to its exceptionally high value of 10.2 mm/yr.

AF demagnetization vector plots for typical pilot samples revealed the optimum AF field which removes the viscous component present.

[10] Sedimentary sequences give only RPI, because there is no definitive theoretical model for how a sediment acquires its magnetization. The intensity of the natural remanent magnetization must therefore be normalized by a magnetic parameter that accounts for variations in the concentration of ferromagnetic minerals. Different normalization parameters, such as, anhysteretic remanent magnetization (ARM), magnetic susceptibility, isothermal remanent magnetization (IRM), and saturation isothermal remanent magnetization (SIRM) are employed in various studies. For the majority of the records considered, RPI is determined by the ratio NRM/ARM after some AF demagnetization (generally between 10 mT and 20 mT) or over several demagnetization steps. *King et al.* [1983] and *Tauxe* [1993] suggested criteria that paleointensity determinations should meet in order to be considered as reliable. These criteria include consistency between the records from a given region, internal agreement between cores, uniform magnetic mineralogy, i.e., concentration variations should be less than an order of magnitude, stable magnetic carriers, same magnetic mineralogy throughout the core, and agreement among different normalization methods.

[11] Another important factor influencing recording fidelity of sediments is the sedimentation rate. The true geomagnetic signal becomes significantly smoothed when the sedimentation rate is decreased [cf. *Roberts and Winklhofer*, 2004]. Usually, an assumption of constant (or piecewise constant) sedimentation rate is made in order to obtain an age model for the whole sediment sequence, with linear interpolation based on only a few tie point ages. In most of the original lake sediment publications only average sedimentation rates are reported. If more information has been provided we calculated a mean value for the sedimentation rate using the age model provided. In Figure 2 we plot a histogram of the average sedimentation rates for the records studied. Lake Aral is a notable outlier with an exceptionally high mean sedimentation of 10.2 mm/yr, due to the tectonic activity, and for clarity of presentation it is excluded from Figure 2. The remainder of the sediment sequences have accumulation rates in the interval of 0.14 to 3.9 mm/yr.

[12] An a priori smoothing time can therefore be estimated for each sediment record based on a lock-in depth and the mean sedimentation rate:

$$\mathrm{T_s} = \frac{\text{lock} - \text{in depth [mm]}}{\text{sedimentation rate [mm/yr]}} \tag{1}$$

A lock-in depth of 100 mm below the surface mixed layer is assumed [cf. *Roberts and Winklhofer*, 2004]. These a priori smoothing times provide a useful minimum thresholds for the time resolution allowed in our spline models described in section 3.2.

3. Robust Smoothing Spline Modeling for Uncertainty Estimates

[13] For a given record (t_i, y_i), where t_i is the age and y_i is an observation, we define a model function $f(t_i)$, such that:

$$y_i = f(t_i) + \epsilon_i; \quad i = 1, 2, \ldots, N \tag{2}$$

where ϵ_i is assumed to be a random, uncorrelated noise. Our aim is to find the smoothest possible function $f(t)$ that satisfactorily fits the observations y_i.

[14] The quality of each individual component, i.e., declination, inclination and RPI, can exhibit different uncertainties due to peculiarities of the coring and acquisition processes. For example, due to possible rotations during the coring, inclination records are often found to be more reliable than the declination records. For this reason, we study each individual field component separately.

3.1. Spline Smoothing Methodology

[15] Cubic spline interpolation is a useful technique for obtaining an interpolation curve between known data points that has desirable stability and smoothness characteristics. It involves constructing a polynomial of low degree between pairs of specified points, known as control points or knots [*Wahba*, 1990]. It has been shown to yield better results than global interpolation, which uses a single function to fit all the data points. The knot points can be identical with the measurement points, but in general this need not be the case. We choose a regular array of knot points with a fixed 50 year spacing, except for a small number of records with a very small a priori smoothing time, in which case a knot spacing of 25 years was adopted. B splines [*de Boor*, 2001] of order four, i.e., cubic splines, with continuous second derivatives are used as basis functions and denoted by $B_j(t)$:

$$f(t) = \sum_{j=1}^{N_K} \alpha_j B_j(t) \tag{3}$$

where N_K is the number of knots and α_j are the spline coefficients. B splines are preferred to polynomial interpolations because they are more accurate, can be easily integrated and differentiated, and do not exhibit spurious oscillations that often accompany polynomial interpolation.

[16] A standard penalized smoothing spline estimation involves minimization of the following objective functional Θ [*Constable and Parker*, 1988], consisting of the L_2 misfit

to the data and a roughness measure defined to be the quadratic norm of the second time derivative

$$\Theta = \sum_{i=1}^{N} [y_i - f(t_i)]^2 + \lambda \int_{t_1}^{t_N} \left[\partial_t^2 f(t)\right]^2 dt \quad (4)$$

where $\lambda > 0$ is a smoothing parameter controlling the trade off between the smoothness and the goodness of fit to the data. This parameter is not specified directly but can be chosen using the method of cross validation (CV) (see section 3.2). t_1 is the start time of the model and t_N is the end time. Due to the presence of non-Gaussian noise and suspected outliers in sediment magnetic records, we instead adopt a 'robust' formulation of the smoothing spline replacing the functional (4) by

$$\Theta = \sum_{i=1}^{N} |y_i - f(t_i)| + \lambda \int_{t_1}^{t_N} \left[\partial_t^2 f(t)\right]^2 dt \quad (5)$$

where the first term is now a L_1 norm of the residuals [e.g., *Menke*, 1989; *Parker*, 1994; *Gubbins*, 2004; *Aster et al.*, 2005; *Tarantola*, 2005]. Using the L_1 norm criterion, i.e., least-absolute deviation, has been shown to reduce the influence of spurious data points, giving them less weight than the L_2 norm [*Claerbout and Muir*, 1973; *Walker and Jackson*, 2000]. Equation (5) can be written in matrix notation as follows:

$$\Theta = \|\mathbf{y} - \mathbf{Bm}\|_1 + \lambda \mathbf{D} \quad (6)$$

where $\mathbf{B}$ is a matrix of B spline construction factors, $\mathbf{m}$ is a matrix of the spline coefficients, $\mathbf{D}$ a matrix of inner products of second derivatives of B splines and $\mathbf{r} = \mathbf{y} - \mathbf{Bm}$ is the residual vector. Minimization of the L_1 norm is carried out by solving a sequence of weighted least squares problems. The solution is obtained by an iterative procedure that involves repeatedly solving the following system [*Schlossmacher*, 1973; *Farquharson and Oldenburg*, 1998]:

$$\left(\mathbf{B}^T\mathbf{WB} + \lambda\mathbf{D}\right)\mathbf{m} = \mathbf{B}^T\mathbf{Wy} \quad (7)$$

where $\mathbf{W}$ is a diagonal weighting matrix, whose elements are determined from the residuals at the previous iteration as $\mathbf{W} = \sqrt{2}/\mathbf{r}$ [e.g., *Walker and Jackson*, 2000], starting with $\mathbf{W}_0 = \mathbf{I}$, where $\mathbf{I}$ is the identity matrix. After solving the normal equations via Cholesky decomposition and determining an appropriate smoothing parameter, where possible using the CV method, we calculate the residuals from the final spline model. Following *Bard* [1974], appropriate L_1 and L_2 measures of the misfit for each element, declination, inclination, or RPI are

$$\sigma_1 = \frac{\sqrt{2}}{N} \sum_{i=1}^{N} |y_i - f(t_i)| \quad (8)$$

and respectively

$$\sigma_2 = \sqrt{\frac{1}{N} \sum_{i=1}^{N} [y_i - f(t_i)]^2} \quad (9)$$

Once a spline model is constructed, it is useful to analyze the model's temporal resolution [e.g., *Constable and Parker*, 1988; *Korte and Constable*, 2008]. This procedure involves inverting a delta function input at various locations with the same smoothing parameter used to create the model [e.g., *Parker*, 1994]. The output is effectively a resolving kernel that diagnoses the amount of smoothing inherent in the spline model. The width at half maximum height of the resolving kernel is thus a measure of the time scale that can be resolved in the record (i.e., it provides the a posteriori estimate of the smoothing time derived from the spline models) and is hereinafter denoted as T_{ss}. We calculate T_{ss} on the internal points of the record, but in Table 1 report only its mean value, which is used for the comparisons in section 3.2. The smoothing time is difficult to derive directly because it depends on the smoothing parameter, the uneven distribution of data, and different weights that are applied to individual points (due to the L_1 measure of misfit).

3.2. Selection of the Smoothing Parameter

[17] The smoothing parameter λ should, where possible, be chosen in an objective way. One well-known automatic procedure for estimation of the smoothing parameter is the method of cross validation (CV) (see *Green and Silverman* [1994] and *Wahba* [1990] for a description and applications). The idea behind this method is the prediction of each data point in turn, using all the remaining data points to find a model that best reproduces the omitted point. It involves making one inversion for each data point, with that data point omitted and then computing the prediction misfit while varying λ. Finally, the λ with the smallest value of cumulative misfit for all inversions (called the CV score) is adopted. We used the following L_1 version of the cross-validation method for determination of λ in order to be consistent with the L_1 objective function used in the construction of the smoothing splines

$$CV(\lambda) = \frac{1}{N} \sum_{i=1}^{N} \left| \frac{y_i - f(t_i)}{1 - A_{ii}(\lambda)} \right| \quad (10)$$

where A_{ii} is the so-called hat matrix which maps the vector of observed values to their predicted values, i.e., $f = \mathbf{A}(\lambda)y$ [*Green and Silverman*, 1994]. This robust CV score is the sum of the absolute values of the residuals corrected by a factor $(1 - \mathbf{A}_{ii})$. A drawback of the method is that this function does not always have a unique minimum, so one must be careful to explore a wide range of λ. In practice, it was evident that a constraint on the minimum degree of smoothing should be implemented in order to avoid underestimating the smoothing parameter. We therefore use mean sedimentation rates, which are inferred from the original studies of each record, and an estimated minimum lock-in depth (below the mixed layer) of 10 cm, following *Roberts and Winklhofer* [2004] and *Lund and Keigwin* [1994], in order to estimate a minimum smoothing time (equation (1)). A search over λ is performed across a wide range of values, starting at an upper limit of 10^{10}, and decreasing until a minimum of CV is found or the smoothing time, as deduced by a resolution analysis of the spline model, reaches the minimum a priori smoothing time derived from the sedimentation rate. In approximately 21% of the records studied

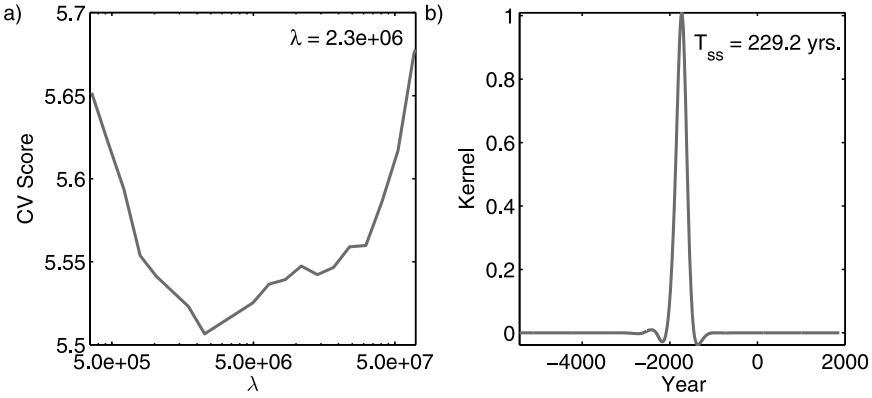

Figure 3. (a) Example of the method of cross validation (CV) for choosing the smoothing parameter (λ) for the relative declination record from Cape Ghir, NW African Margin (GHI). The minimum of the CV score determines the choice of λ. The x axis is given in logarithmic scale. (b) An example of the kernel function on the central point of the same record, which diagnoses a temporal resolution of 229.2 years. The width refers to a full width at half maximum of this kernel function. The robust smoothing spline model for this record is presented in Figure 5 (top).

the smoothing parameter was objectively determined by the CV method. In the remainder it was set by the a priori threshold smoothing time T_s; the unexpectedly low number of objective determinations of λ was partly because some of the records had already been presmoothed, and partly due to the existence of inconsistent cores in some records.

[18] In order to test the influence of the a priori assumed lock-in depth, we performed robust smoothing spline modeling with different example lock-in depths of 5 cm, 10 cm, and 15 cm. The results for the inclination record from Pohjajärvi, Finland (POH), show that σ_2 for the inclination varied by less than one degree, i.e., 2.66°, 2.47°, and 2.50° for 5 cm, 10 cm, and 15 cm depths, respectively. The effect is similar for the declination record, with variations of the order of degree. In the remainder of the study we therefore take a pragmatic approach and implement a constraint based on an assumed lock-in depth of 10 cm. This is sufficient to prevent gross underestimation of the smoothing parameter.

3.3. Results From Robust Spline Modeling

[19] The robust smoothing spline modeling technique was applied to the Holocene sediments records listed in Table 1. In each case the original data set was used without rejection of data. An example of the CV score as a function of the smoothing parameter λ is presented in Figure 3 for the relative declination record of Cape Ghir, NW African Margin (GHI). The minimum of the CV function with respect to λ determines the smoothness of the spline model fitting to the data. Also shown in Figure 3 is the temporal resolution kernel, i.e., the response obtained from the spline model to a delta input, in this case placed on the central data point.

[20] For illustration, robust smoothing spline analysis is demonstrated on two typical examples, where the three components are available, Lago di Mezzano, Italy, and Cape Ghir, NW African Margin, in Figures 4 and 5, respectively. Similar plots for all records are available online from the EarthRef Digital Archive (ERDA) at http://earthref.org/ERDA/1383. If the CV score is used then a label 'not constrained' is added, otherwise the threshold time value determined from the sedimentation rate is stated. The subplots show the data in units of degrees and the robust smoothing spline fit, together with the associated histogram of residuals (normalized to the unit area). To allow comparisons across the records, we work with a standardized version of RPI records, defined as

$$RPI_{stand} = \frac{RPI}{\sqrt{\frac{1}{N}\sum_{i=1}^{N}(RPI_i - \mu)^2}} \tag{11}$$

where $\mu = 1/N\Sigma_{i=1}^{N} RPI_i$ is the mean value.

[21] Overall, we find that the robust spline modeling technique performs well, producing smooth models that explain the most coherent signals in the magnetic records. Outliers do not greatly distort the spline model, while the data gaps are handled in a parsimonious manner without spurious oscillations (e.g., Figures 4 and 5). The histograms of the residuals are typically well explained by a Laplacian distribution, though due to the rather small number of data points it is difficult to rigorously favor either a Gaussian or Laplacian uncertainty model. In sections 4 and 5 we use the variance measure (σ_2, henceforth σ_{rss}, where 'rss' stands for the random error determined from the robust smoothing splines) to characterize the spread in the residuals, since this is easier to combine with other uncertainty estimates. For the records studied, σ_{rss} ranges from 0.5° to 11.6° (median value: 2.7°; interquartile range: 1.8° to 4.4°) for inclination, 1.2° to 45.6° (median value: 7.5°; interquartile range: 5.1° to 13.2°) for declination, and 0.2 to 1.0 (median value: 0.5; interquartile range: 0.3 to 0.6) for standardized RPI. The smoothing times T_{ss} inferred from the spline modeling range from 27 to 980 years with a median value of 130 years and an interquartile range from 80 to 250 years. The distribution of the a posteriori smoothing times T_{ss} is presented in Figure 6. Results for σ_{rss} and T_{ss} for all lakes are reported in Table 1. The large spread of values obtained for σ_{rss} and T_{ss}, and the significant differences between components, demonstrates the importance of considering each

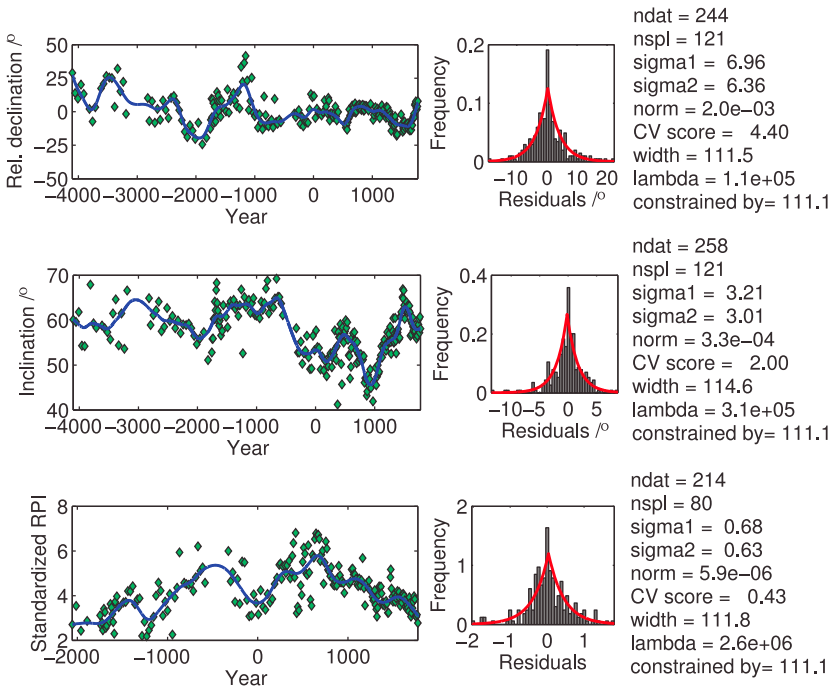

Figure 4. Example of the robust spline analysis of (top) relative declination, (middle) inclination, and (bottom) standardized relative paleointensity data from Lago di Mezzano, Italy. Also shown are the histograms of the residuals (normalized to the unit area) with a Laplacian distribution with mean and deviation calculated from the residuals. Information about the number of data (ndat), the number of splines functions used (nspl), the L_1 measure of misfit σ_1 (sigma1), the L_2 measure of misfit σ_2 (sigma2), the norm measuring the model roughness (norm), the value of the CV minimum (CV score), the width of the resolving kernel or T_{ss} (width), the corresponding smoothing parameter λ (lambda), and a priori smoothing time T_s (constrained by) is provided in the legends on the right.

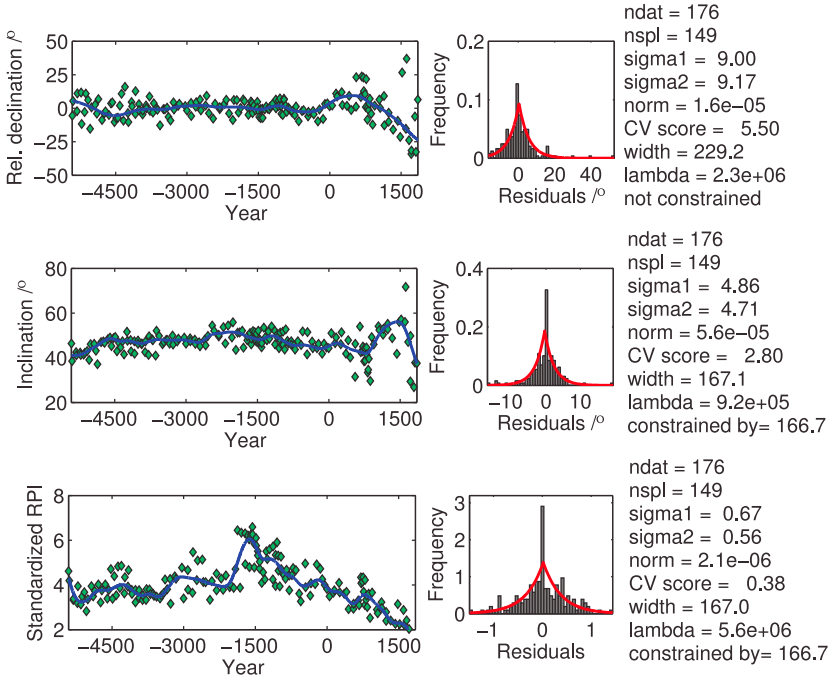

Figure 5. Example of the robust spline analysis of (top) relative declination, (middle) inclination, and (bottom) standardized relative paleointensity data from Cape Ghir, NW African Margin. Also shown are the histograms of the residuals (normalized to the unit area) with a Laplacian distribution with mean and deviation calculated from the residuals. An explanation of the labels is given in Figure 4.

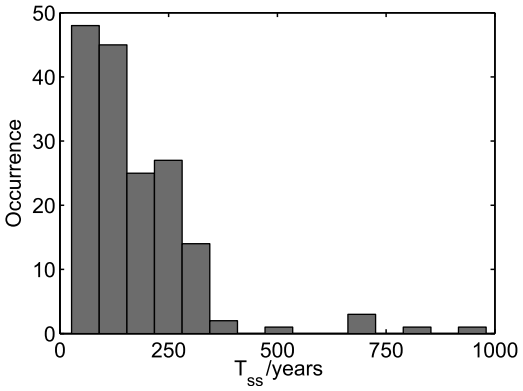

Figure 6. Histogram of the a posteriori smoothing time T_{ss} obtained from the smoothing spline modeling for relative declination, inclination, and RPI of the Holocene sediment records.

component of each record separately when deriving uncertainty estimates.

4. Comparison of Lake Sediments With Other Recorders and Global Models

[22] In addition to the spline modeling analysis, we carried out comparisons between the database of Holocene sediment magnetic records and nearby archeomagnetic data, other nearby lake sediments, the historical field model *gufm*1 in the time periods of overlap, and the archeomagnetic field model ARCH3k.1 when nearby archeomagnetic data are available. Where possible, these comparisons enable an independent assessment of the fidelity of sediment records that include the effects of both random and also systematic uncertainties that could not be assessed by the spline modeling. In order to assess the difference between the compared quantities for each record, we use the following L_2 measure

$$\sigma_c = \sqrt{\frac{1}{N_c}\sum_{i=1}^{N_c}[y_i - \hat{y}(t_i)]^2} \qquad (12)$$

where $\hat{y}$ are either 'neighboring' archeomagnetic or lake records, or else global model predictions and N_c is the number of the compared data points. 'Neighboring' is defined as within 5° latitude and longitude from the record location; such neighbors were then relocated to the lake location using the CALS7k.2 model [*Korte and Constable*, 2005], which is a minor correction of at most 2%. In some cases, the compared values are not of exactly the same age. In this case the mean value of sediment record within an interval of ±50 years was used for the comparison. In the case of neighboring records, σ_c is computed as a mean over all the data available for comparison with a particular record. We report the results of comparisons only when 30 or more data were available for the comparison, in order to obtain statistically reliable estimates. The quantity of comparisons with the historical field model *gufm*1 is unfortunately small because of the short period of overlap. Moreover, the magnetization of the top of sediment cores may be not locked in, which may result in inconsistency when attempting to compare magnetic sediment records with the *gufm*1.

[23] In the comparisons we also use RPI in the standardized form defined in equation (11). Furthermore, due to the fact that many cores may not have been oriented to a known azimuth, we also compare declination values in terms of the deviation from the average value of the record, i.e., we consider $D_{rel} = D_{obs} - 1/N \sum_{i=1}^{N} D_{iobs}$. Absolute inclination values are however considered. The lack of absolute measurements of declination and paleointensity from the lake sediments requires a special calibration technique. Calibration involves addition of a constant for relative declination and a multiplication by a scaling factor for RPI, respectively. We choose to consider each absolute datum, i.e., field model prediction or archeomagnetic datum, in turn to be the true absolute value of the field, and calibrate the entire lake sediment record by assuming the lake estimate and the selected datum agree at that time. The remaining absolute data can then be compared to the calibrated sediment record. This process is repeated for all the available absolute data M and the total number of comparisons in this case is $N_c = M(M - 1)$. The variance σ_c is then obtained from all the comparisons using equation (12). Examples of such comparisons are presented in Figure 7, where the relative declination, inclination and standardized RPI time series from Lago di Mezzano (Italy), the *gufm*1 and ARCH3k.1 predictions, and archeomagnetic data are presented.

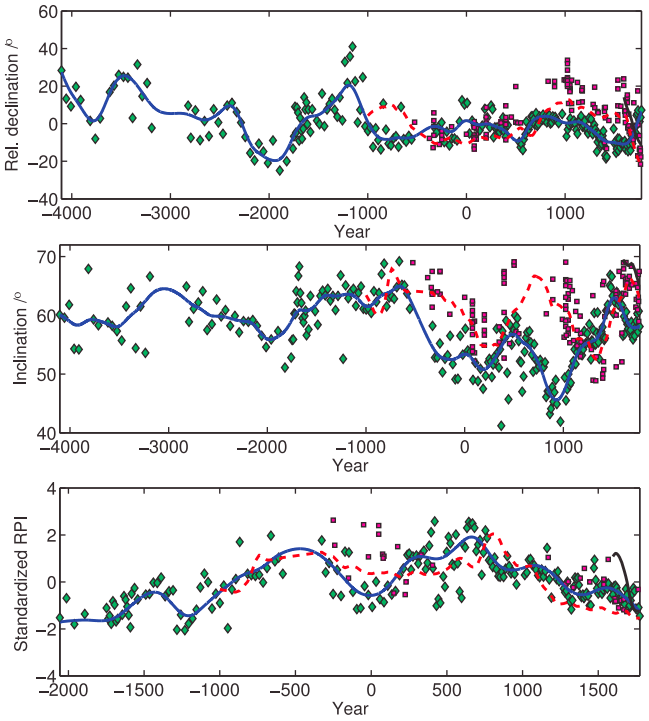

Figure 7. Examples of the comparisons between lake sediment data from Lago di Mezzano, Italy (green diamonds), global field models *gufm*1 (black curve) and ARCH3k.1 (red dashed curve), and archeomagnetic data (red squares). Robust smoothing spline fit (blue curve) is shown for reference. Declinations are presented as deviations from their mean value, while RPI are standardized according to the mean and the standard deviation.

Table 2. Minimum, Maximum, and Median Values and Interquartile Ranges From Comparison Between Holocene Sediment Database and the Historical Geomagnetic Field Model *gufm1*, the ARCH3k.1 Global Model, Archeomagnetic Data, and Nearby Lake Sediment Records

Comparison[a]	Component	n[b]	Minimum	Maximum	Median	Interquartile Range
gufm1	σ_c Inclination (deg)	8	2.2	17.1	7.0	6.3 to 9.8
	σ_c Declination (deg)	6	12.7	34.2	21.8	18.0 to 27.5
	σ_c RPI	1	1.4	1.4	1.4	1.4 to 1.4
	β_c Inclination (deg)	8	−8.3	16.2	−3.1	−5.9 to −0.5
ARCH3k.1	σ_c Inclination (deg)	17	3.2	8.1	5.7	5.0 to 6.8
	σ_c Declination (deg)	15	5.2	24.6	9.6	7.6 to 21.7
	σ_c RPI	3	0.7	1.4	1.3	0.7 to 1.4
	β_c Inclination (deg)	17	−6.4	6.3	−0.9	−4.0 to 2.3
Archeomagnetic data	σ_c Inclination (deg)	18	5.0	9.9	7.6	6.6 to 8.2
	σ_c Declination (deg)	16	10.0	27.8	17.7	13.6 to 23.8
	σ_c RPI	5	1.2	2.8	1.5	1.3 to 2.7
	β_c Inclination (deg)	18	−7.3	6.1	0.1	−4.4 to 3.6
Nearby lakes	σ_c Inclination (deg)	49	3.1	14.7	7.6	6.5 to 10.8
	σ_c Declination (deg)	45	8.0	151.2	18.4	14.4 to 27.9
	σ_c RPI	17	1.0	3.8	1.7	1.4 to 2.5
Uncertainty estimates[c]	σ_l Inclination (deg)	72	2.5	11.2	5.9	5.4 to 7.2
	σ_l Declination (deg)	68	4.1	46.9	13.4	11.4 to 18.9
	σ_l RPI	27	0.59	1.32	0.93	0.86 to 1.01

[a]The Holocene sediment database was compared to the ARCH3k.1 global model only when nearby archeomagnetic data were available. σ_c is obtained using equation (12), and β_c is systematic bias, which can only be assessed for inclination.
[b]n is the number of comparisons considered, each of which has more than 30 contributing data.
[c]Last three rows are the final uncertainty estimates obtained by combination of errors (see section 5).

[24] The *gufm*1 and ARCH3k.1 field models are used for the comparisons since they are truly independent of the lake sediment data. Their predictions do not always provide a good fit to the sediment records, and offsets in magnitude and time shifts are observed (e.g., Figure 7). Residuals from the comparisons exhibit in some cases positive or negative mean biases, indicating systematic shifts between the compared quantities. The offsets in inclination obtained by the comparison with the archeomagnetic data and ARCH3k.1 field model (when archeomagnetic data exist) however show no conclusive evidence for systematic inclination shallowing across the compilation of records studied here. For instance, the offsets obtained in the comparisons with the ARCH3k.1 model (when nearby archeomagnetic data were available) range from −6.4° to 6.3° (interquartile range: −4.0° to 2.3°) with a median of −0.9°. The range (minimum and maximum value) together with the median and interquartile values from the four types of comparisons are summarized in Table 2. Considering all comparisons, a much better agreement is found for inclination than for declination data. Comparison of inclination estimates yields similar results in all four cases, with median values of σ_c of between 5° and 8°. Encouragingly, good results are obtained for the inclination comparisons between nearby records, indicating a strong interlake consistency of inclination. The best comparison results for declination are achieved when lake sediments data are compared with the ARCH3k.1 model when nearby archeomagnetic data are available; see Table 2. The maximum value for relative declination comparison with nearby records is obtained between the two coring sites in Arctic Ocean (Alaskan margin and Chukchi Sea), where sharp declination changes with very high amplitudes occur in both records. Overall, these comparisons again indicate the wide range of fidelities that occur in Holocene sediment records and how it is essential to have individual uncertainty estimates for each component of each record.

[25] From these test results, we conclude that the most useful comparisons of the sediment records are with the ARCH3k.1 model evaluated at times when archeomagnetic data are available in a region close to the lake site (within ±5° latitude and longitude). Comparison with *gufm*1 is limited by the short period of overlap and by atypical behavior at the top of many sediment cores. Comparison with other sediment records is complicated by the fact that we do not have independent a priori estimates of the accuracy of the other sediment records. Direct comparisons with archeomagnetic data are also difficult due to the considerable scatter that is sometimes present in these measurements. In contrast, the ARCH3k.1 model provides a parsimonious estimate of the field at the location of interest that is compatible with nearby archeomagnetic samples, independent from sediment records. Because the records span several thousand years they enable many comparisons. Note again that we make these comparisons only when nearby archeomagnetic data are available, that is at times when ARCH3k.1 is well constrained by observations. A further advantage of this approach is that uncertainty estimates are available for the model predictions [*Korte et al.*, 2009], which is useful for the combination of uncertainties considered in section 5. Henceforth, we use the terminology 'archeomagnetic estimate' (X_a) to mean the prediction from the ARCH3k.1 model estimated at the record location.

5. Uncertainty Estimates for Global Field Modeling

[26] In order to construct reliable models of the geomagnetic field, consistent and independent uncertainty estimates

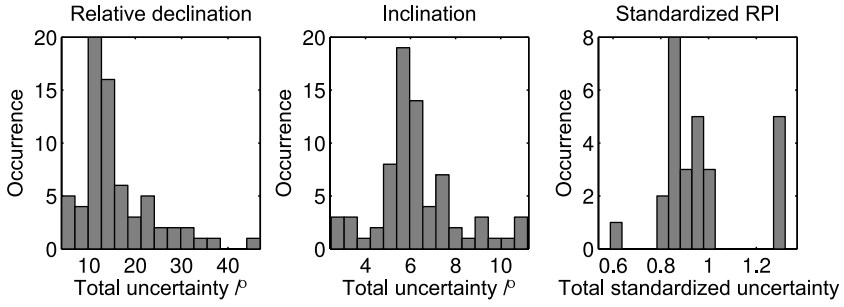

Figure 8. Histograms summarizing our estimated uncertainties for Holocene sediment magnetic records.

are required. The structure of an uncertainty may generally be divided into random and systematic. Random uncertainties are assumed to involve fluctuations around the true value while systematic uncertainties deviate from the truth in a predictable manner. It is important when considering the uncertainty in sediment records to use estimates that encompass both random and possible systematic contributions. By fitting a robust smoothing spline model and looking at the variance of the data away from the resulting smooth curve, we have obtained a measure of the random variability present in each record. The comparative analysis (e.g., with archeomagnetic estimates), on the other hand provides a means to assess the total uncertainty, including both random and also any systematic uncertainty that may be present.

[27] Following *Rice* [1995], we can write the true value of a quantity X as a sum of a measurement x_0, the systematic β and the random ϵ components of the uncertainty, with an expected value $E(\epsilon) = 0$ and a variance $Var(\epsilon) = \sigma^2$

$$X = x_0 + \beta + \epsilon; \quad E(X) = x_0 + \beta; \quad Var(X) = \sigma^2 \tag{13}$$

The estimated uncertainty is then the expected squared deviation of the true value from the measurement

$$E\left[(X - x_0)^2\right] = \sigma^2 + \beta^2 \tag{14}$$

which represents the sum of the systematic bias and the random variance. For the lake sediment records we adopt the following related model

$$X_l = x_l^{true} + \beta_l + \epsilon_l^{rss} + \epsilon_l^{add} \tag{15}$$

where β_l is any systematic bias present in the sediment record and the random uncertainty ϵ_l is separated into two components. The ϵ_l^{rss} which is a random uncertainty that we estimate from the variance of sediment data about our robust spline models, which have variance $Var[\epsilon_l^{rss}] = \sigma_{rss}^2$. The term ϵ_l^{add} then represents additional random uncertainty that we cannot assess by looking at deviations from a spline fit, e.g., due to uncertainties in the age model; this component is allocated a variance $Var[\epsilon_l^{add}] = \sigma_{add}^2$. Using this model, the estimated uncertainty for a sediment record is:

$$\sigma_l^2 = \beta_l^2 + \sigma_{rss}^2 + \sigma_{add}^2 \tag{16}$$

Comparisons X_c between the sediment data X_l and archeomagnetic estimates X_a, where $X_c = X_l - X_a$, involve uncertainties of both contributing quantities, i.e.,

$$\beta_c^2 + \sigma_c^2 = \beta_l^2 + \sigma_{rss}^2 + \sigma_{add}^2 + \beta_a^2 + \sigma_a^2 \tag{17}$$

where β_c and σ_c are now the systematic bias and variance, respectively, of the comparison residuals, and β_a and σ_a are the bias and variance of the archeomagnetic estimates. For a given record, we take σ_a from the root mean square of the uncertainties predicted by the ARCH3k.1 model for each comparison; these uncertainties are based on parametric bootstrap resampling techniques [*Korte et al.*, 2009]. The systematic bias β_a of the archeomagnetic estimates are neglected, since its magnitude is found to be small based on direct comparisons between archeomagnetic data and *gufm*1 model (the median values are $-1°$ for inclination, $0.3°$ for declination and -0.8 μT for the intensity). The systematic bias of the comparison for inclination can then be ascribed only to the bias of sediment records, i.e., $\beta_l = \beta_c$. On the other hand the bias cannot be determined from the comparisons of relative declination and RPI.

[28] We must consider two possible cases:

[29] 1. For lakes with sufficient comparisons to archeomagnetic estimates (i.e., there is sufficient nearby archeomagnetic data), our final uncertainty estimate is based on the uncertainty estimates from the comparisons and the archeomagnetic estimates, i.e., $\sigma_l^2 = \sigma_c^2 - \sigma_a^2 + \beta_c^2$ for inclination, $\sigma_l^2 = \sigma_c^2 - \sigma_a^2$ for the declination, and standardized RPI.

[30] 2. When no or few (less than 30) archeomagnetic estimates are available for comparison, mean values for σ_{add} and β_l are used, as calculated from cases when comparisons were possible, utilizing the expression $\sigma_{add}^2 = \sigma_c^2 - \sigma_{rss}^2 - \sigma_a^2$. Then, following equation (16), these are combined with σ_{rss}^2 for the particular record to obtain the required uncertainty estimates. In cases when the term $(\sigma_c^2 - \sigma_a^2)$ is smaller than σ_{rss}^2 then no additional uncertainty is assigned, i.e., $\sigma_{add}^2 = 0$. This approach therefore combines information specific to each record derived from the spline analysis, with mean values obtain from comparisons with archeomagnetic estimates.

[31] Final uncertainty estimates σ_l for each record are listed in Table 1. To convert our standardized RPI uncertainty estimates to absolute intensity uncertainty estimates, the standard deviation of the RPI can be multiplied by a preferred scaling factor for the record of interest [cf. *Korte and*

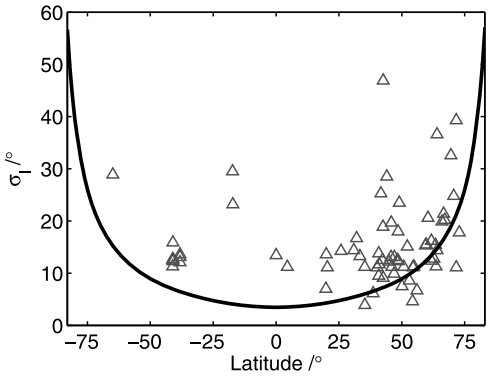

Figure 9. Dependence of uncertainty estimates for declination σ_I on latitude. Triangles are our uncertainty estimates for relative declination. The solid line represents the values estimated using equation (2) from *Donadini et al.* [2009], where σ_I depends on the local inclination. Here, the inclination is obtained from the Geocentric Axial Dipole hypothesis and α_{95} = 6°, the threshold value used for the uncertainty estimates in the lake sediment records by *Donadini et al.* [2009]. The exceptions (EAC, BAR, and LOU) are declination records with anomalously large data scatter.

Constable, 2006]. Histograms of the uncertainty estimates obtained for all lakes are plotted in Figure 8. They show a wide range of uncertainty estimates across the lakes studied, spanning 2.5° to 11.2° for inclination (interquartile range: 5.4° to 7.2°), 4.1° to 46.9° for relative declination (interquartile range: 11.4° to 18.9°) and 0.59 to 1.32 (interquartile range: 0.86 to 1.01) for the standardized RPI.

6. Discussion

[32] The primary goal of this study was to assess the quality of Holocene sediment magnetic records and to provide individual weightings to be used in future geomagnetic field model construction. *Nilsson et al.* [2010] previously found that poor quality paleomagnetic data and large dating uncertainties force complex models to place too much power into higher degrees. With reliable and consistent errors allocated to individual data sets it may therefore be possible for simpler models to adequately explain the variance in many of the records.

[33] In the study of *Korte et al.* [2005], minimum uncertainties for lake sediment records based on comparisons with *gufm*1 were predominantly used. Default uncertainties of 3.5° in inclination, 5.0° in declination and 5 μT in intensity were allocated. *Donadini et al.* [2009] expressed their minimum uncertainty estimate in terms of a minimum α_{95} of 6°, which corresponds to a 3.5° uncertainty in inclination, with declination uncertainties depending on the inclination at the location. In contrast, our analysis suggests a wider range of uncertainties that differ greatly between inclination and declination. We find inclination uncertainties with a median value of 5.9° and an interquartile range of 5.4° to 7.2°; thus we would allocate uncertainties at most lakes that are considerably larger than the threshold values used by *Korte et al.* [2009] and *Donadini et al.* [2009]. Our uncertainty estimates for relative declination have a median value of 13.4° and an interquartile range of 11.4° to 18.9°, much larger than the previously considered uncertainties. For comparisons with previous studies the standardized RPI uncertainty estimates first need to be calibrated to an absolute scale, multiplying by the standard deviation and a rescaling factor specific for each record. Performing such a calibration using the CALS7k.2 field model, we obtain absolute uncertainty estimates for the paleointensity with a median value of 11 μT and an interquartile range of 9 to 14 μT. For all three components, we arrive at uncertainty estimates, that are much larger than those used previously. Our uncertainty estimates implicitly include the effect of age uncertainties while the uncertainties quoted from the previous studies [*Korte et al.*, 2005] do not. However if the age uncertainties proposed by *Korte et al.* [2005] are mapped into measurement uncertainties they equate to a relatively small contribution [see *Korte et al.*, 2005, Table 5].

[34] A different approach to account for age uncertainties is used in the more recent global models of the geomagnetic field CALS3k.3, CALS3k.4 and CALS10k [*Korte and Constable*, 2008; *Korte et al.*, 2009; *Korte and Constable*, 2011; *Korte et al.*, 2011]. They created multiple possible solutions by bootstrap resampling of a statistical model for age uncertainties, in such a way that the record can be shifted in time by ±300 years. A similar approach is applied to the uncertainties of magnetic components, where each bootstrap sample is obtained from a normal distribution centered on the magnetic component with a standard deviation equal to the data uncertainty estimate. Thus, an average of all bootstraps hopefully provides a robust picture of the field structure. Nevertheless, this technique relies on the error estimates being allocated to each record [*Donadini et al.*, 2009]. In particular our results suggest this should be done on a lake by lake basis, which has not previously been the case.

[35] We find the largest uncertainties in inclination in cases where there is much scatter in the data or many outliers are present, e.g., Lake Barrine, Australia (σ_I = 10.9°), Lake Fangshan, China (σ_I = 11.2°), Hoya de San Nicolas, Mexico (σ_I = 11.3°) and Lake Eacham, Australia (σ_I = 10.4°). The smallest uncertainties in inclination are observed in consistent records, usually when uncertainties are estimated via comparison with archeomagnetic estimates, e.g., Lake Begoritis, Greece (σ_I = 2.5°) and Lac du Bourget, France (σ_I = 2.9°). The Lake Biwa record showed the smallest uncertainty estimate for declination (σ_I = 4.1°) but this is probably an artifact due to presmoothing of the record, which yields not only an unrealistically small random uncertainty, but also limits the uncertainties derived from comparisons. Declination uncertainty estimates tend to increase with latitude (Figure 9). The approach used by *Donadini et al.* [2009] also allows a similar dependence of the declination uncertainty with location, i.e., local inclination. Our uncertainty estimates follow the trend expected with their technique (see Figure 9), the few exceptions are declination records with anomalously large data scatter. In general, there are no obvious geographical regions with characteristically smaller or larger uncertainty estimates found across all components. An exception is that many of the best declination records come from Europe, for example, Lake Windermere (σ_I = 5.8°), Loch Lomond (σ_I = 9.3°) and Llyn Geirionydd (σ_I = 8.8°) in UK; Lake Trikhonis (σ_I = 6.8°) and Lake Begoritis (σ_I = 9.4°) in Greece; Eifel maars, Germany (σ_I = 8.3°), but there are also lakes with

larger uncertainty estimates in this region, for example, Lac d'Annecy, France (σ_I = 21.5°), Meerfelder Maar, Germany (σ_I = 24.5°) and Sarsjön, Sweden (σ_I = 36.6°). In general, as pointed out by a reviewer, these results imply that the uncertainties have not reduced over time, in fact one of the best studies (in terms of our uncertainty estimates) remains the early study by *Turner and Thompson* [1981]. In spite of the development of equipment and instrumentation, recent records are not necessarily more reliable than older records. While in the past, the studies were focused on obtaining paleosecular variation data, today paleomagnetic studies are not always the first priority, i.e., the sites are usually not selected exclusively for secular variation purposes.

[36] During this analysis, several difficulties were encountered related to the heterogeneous form in which lake sediment data are available. First, records whose data was provided in presmoothed form (e.g., Aral Sea, Kazakhstan, Lake Aslikul, Russia, Lake Biwa, Japan, Lake LeBoeuf, USA, Lake Windermere, UK, Gardar Drift, N. Atlantic, Finnish Lakes) resulted in unrealistically small estimates of σ_{rss}. We recommend that in the future, records should be published and contributed to databases in raw, unsmoothed, form. Smoothed versions can still be presented as well, but the raw form is essential for further modeling. In this way information about the inherent reliability of records is preserved. Second, records consisting of multiple cores that are subsequently mixed or stacked together (e.g., Lac d'Annecy, France; Lake Huron, USA) produced much larger, and probably more realistic, uncertainty estimates. However, before using such records for field modeling, it may be preferable to reject cores that are incompatible with data from other sources (e.g., archeomagnetic data, nearby lake records or other cores from the same lake). This requires that data from individual cores are separately included in databases along with their depth-age model. Third, high-latitude records, such as those from Arctic and Antarctic seas, are found to possess a large random variance of declination due to rapid, large amplitude directional changes in these regions; it is essential that these records are given dedicated, suitably large, uncertainty estimates in field modeling. Fourth, our results from the comparisons show no evidence for systematic shifts between lake sediment inclination data and archeomagnetic estimates. Caution should be exercised when automatically correcting the inclination shallowing without having any direct evidence for it in the records. Fifth, cores oriented to an azimuth should be collected whenever possible, or at least the upper sediments should be matched to measured local declination. Oriented data would help improve future geomagnetic field models, particularly at high latitudes.

[37] In this study we have not separately accounted for age uncertainties; instead, these are included within the comparison uncertainties, in particular contributing to the factor σ_{add}. Future studies may wish to use a more sophisticated approach that treats age uncertainties separately or try to determine shift factors associated with age problems during the field modeling procedure.

7. Conclusion

[38] In this study we have provided new, individually tailored, uncertainty estimates for the magnetic records from Holocene sediments. These were derived from comparisons with archeomagnetic estimates and from the scatter about robust smoothing spline models. The uncertainties obtained span a wide range of values, demonstrating the diversity in quality of the records. Holocene sediment magnetic records are clearly very heterogeneous, with the amount of data scatter and the degree of time averaging depending both on the acquisition process and the experimental protocol used to obtain paleomagnetic data. Our new uncertainty estimates have median values larger than the threshold uncertainty estimates allocated in previous studies. Rather than using nominal uncertainty estimates for most lakes, we propose that individual uncertainty estimates are necessary for field modeling. We find inclination records to be the most accurate and reliable form of magnetic data presently available from Holocene sediments. No evidence for systematic inclination shallowing is found from our comparison analysis. Due to problems during recovery of cores we suggest that only relative variations in declination are used in field modeling. Study of the temporal resolution of the spline models for each record indicates similar heterogeneity, with smoothing times with an interquartile range of 80 to 250 years. This suggests it should be possible to study secular variation processes with time scales of about 100 to 1000 years with lake sediments records, provided the sedimentation rate is sufficiently fast, and the record is of sufficiently long duration.

[39] **Acknowledgments.** We thank M. Korte for making her database of Holocene lake sediment magnetic records available and A. Jackson for discussions regarding the cross-validation method. We also thank C. Constable and an anonymous reviewer for their constructive suggestions for improving the manuscript. The research was supported by the CHIRP1 project of ETH (CH1-02-08-2).

References

Ali, M., H. Oda, A. Hayashida, K. Takemura, and M. Torii (1999), Holocene palaeomagnetic secular variation at Lake Biwa, central Japan, *Geophys. J. Int.*, *136*, 218–228.

Aster, R., B. Borchers, and C. Thurber (2005), *Parameter Estimation and Inverse Problems*, Elsevier Acad., Amsterdam.

Bard, Y. (1974), *Nonlinear Parameter Estimation*, Academic, New York.

Barletta, F., G. St-Onge, J. Channell, A. Rochon, L. Polyak, and D. Darby (2008), High-resolution paleomagnetic secular variation and relative paleointensity records from the western Canadian Arctic: Implication for Holocene stratigraphy and geomagnetic field behaviour, *Can. J. Earth Sci.*, *45*, 1265–1281.

Barton, C., and M. McElhinny (1981), A 10 000 yr geomagnetic secular variation record from three Australian maars, *Geophys. J. R. Astron. Soc.*, *67*, 465–485.

Barton, C., and T. Torgersen (1988), Palaeomagnetic and ^{210}Pb estimates of sedimentation in Lake Turkana, East Africa, *Palaeogeogr. Palaeoclimatol. Palaeoecol.*, *68*, 53–60.

Bleil, U., and M. Dillon (2008), Holocene Earth's magnetic field variations recorded in marine sediments of the NW African continental margin, *Stud. Geophys. Geod.*, *52*, 133–155.

Boudreau, B. (1994), Is burial velocity a master parameter for bioturbation?, *Geochim. Cosmochim. Acta*, *58*, 1243–1249.

Boudreau, B. (1998), Mean mixed depth of sediments: The wherefore and the why, *Limnol. Oceanogr.*, *43*, 524–526.

Brachfeld, S., and S. Banerjee (2000), A new high-resolution geomagnetic relative paleointensity record for the North American Holocene: A comparison of sedimentary and absolute intensity data, *J. Geophys. Res.*, *105*, 821–834.

Brachfeld, S., G. Acton, Y. Guyodo, and S. Banerjee (2000), High-resolution paleomagnetic records from Holocene sediments from the Palmer Deep, Western Antartic Peninsula, *Earth Planet. Sci. Lett.*, *181*, 429–441.

Brachfeld, S., E. Domack, C. Kissel, C. Laj, A. Leventer, S. Ishman, R. Gilbert, A. Camerlenghi, and L. Eglinton (2003), Holocene history

of the Larsen-A Ice Shelf constrained by geomagnetic paleointensity dating, *Geology*, *31*, 749–752.

Brandt, U., N. Nowaczyk, A. Ramrath, A. Brauer, J. Mingram, S. Wulf, and J. Negendank (1999), Palaeomagnetism of Holocene and Late Pleistocene sediments from Lago di Mezzano and Lago Grande di Monticchio (Italy): Initial results, *Quat. Sci. Rev.*, *18*, 961–976.

Brown, H. (1991), A palaeomagnetic, geochronological, and palaeoenvironmental investigation of late and postglacial maar lake sediments from NW Europe, Ph.D. thesis, Univ. of Edinburgh, Edinburgh, U. K.

Channell, J. E. T., and Y. Guyodo (2004), The Matuyama Chronozone at ODP Site 982 (Rockall Bank): Evidence for decimeter-scale magnetization lock-in depths, in *Timescales of the Paleomagnetic Field*, *Geophys. Monogr. Ser.*, vol. 145, edited by J. E. T. Channell et al., pp. 205–219, AGU, Washington, D. C., doi:10.1029/145GM15.

Channell, J., D. Hodell, and B. Lehman (1997), Relative geomagnetic paleointensity and δ^{18}O at ODP Site 983 (Gardar Drift, North Atlantic) since 350 ka, *Earth Planet. Sci. Lett.*, *153*, 103–118.

Chaparro, M. A. E., H. N. Böhnel, R. Byrne, N. R. Nowaczyk, R. S. Molina-Garza, J. Park, and J. F. W. Negendank (2008), Palaeomagnetic secular variation and rock-magnetic studies of Holocene sediments from a maar lake (Hoya de San Nicolas) in central Mexico, *Geophys. J. Int.*, *175*, 462–476.

Claerbout, J., and F. Muir (1973), Robust modeling with erratic data, *Geophysics*, *38*, 826–844.

Constable, C. (1985), Eastern Australian geomagnetic field intensity over the past 14000 yr, *Geophys. J. R. Astron. Soc.*, *81*, 121–130.

Constable, C., and M. McElhinny (1985), Holocene geomagnetic secular variation records from north-eastern Australian lake sediments, *Geophys. J. R. Astron. Soc.*, *81*, 103–120.

Constable, C., and R. Parker (1988), Smoothing, splines and smoothing splines; Their application in geomagnetism, *J. Comput. Phys.*, *78*, 493–508.

Constable, C., C. Johnson, and S. Lund (2000), Global geomagnetic field models for the past 3000 years: Transient or permanent flux lobes, *Philos. Trans. R. Soc. London A*, *358*, 991–1008, doi:10.1098/rsta.2000.0570.

Creer, K., P. Readman, and S. Papamarinopoulos (1981), Geomagnetic secular variation in Greece through the last 6000 years obtained from lake sediment studies, *Geophys. J. R. Astron. Soc.*, *66*, 193–219.

Creer, K., D. Valencio, A. Sinito, P. Tucholka, and J. Vilas (1983), Geomagnetic secular variations 0–14,000 yr BP as recorded by lake sediments from Argentina, *Geophys. J. R. Astron. Soc.*, *74*, 199–221.

de Boor, C. (2001), *A Practical Guide to Splines*, Springer, New York.

Donadini, F., M. Korte, and C. G. Constable (2009), Geomagnetic field for 0–3 ka: 1. New data sets for global modeling, *Geochem. Geophys. Geosyst.*, *10*, Q06007, doi:10.1029/2008GC002295.

Farquharson, C., and D. Oldenburg (1998), Non-linear inversion using general measures of data misfit and model structure, *Geophys. J. Int.*, *134*, 213–227.

Finlay, C. C., et al. (2010), International Geomagnetic Reference Field: The eleventh generation, *Geophys. J. Int.*, *183*, 1216–1230.

Frank, U. (2007), Palaeomagnetic investigations on lake sediments from NE China: A new record of geomagnetic secular variations for the last 37 ka, *Geophys. J. Int.*, *169*, 29–40.

Frank, U., N. Nowaczyk, J. Negendank, and M. Melles (2002a), A paleomagnetic record from Lake Lama, northern central Siberia, *Phys. Earth Planet. Inter.*, *133*, 3–20.

Frank, U., M. Schwab, and J. Negendank (2002b), A lacustrine record of paleomagnetic secular variations from Birkat Ram, Golan Heights (Israel) for the last 4400 years, *Phys. Earth Planet. Inter.*, *133*, 21–34.

Frank, U., M. Schwab, and J. Negendank (2003), Results of rock magnetic investigations and relative paleointensity determinations on lacustrine sediments from Birkat Ram, Golan Heights (Israel), *J. Geophys. Res.*, *108*(B8), 2379, doi:10.1029/2002JB002049.

Frank, U., N. Nowaczyk, and J. Negendank (2007), Palaeomagnetism of greigite bearing sediments from the Dead Sea, Israel, *Geophys. J. Int.*, *168*, 904–920.

Geiss, C., J. Dorale, and D. Dahms (2007), A rockmagnetic and palaeomagnetic record of two glacial lakes in the Wind River Range, Wyoming, USA, *Eos Trans. AGU*, *88*(52), Fall Meet. Suppl., Abstract GP53B-1216.

Gogorza, C., A. Sinito, J. Lirio, H. Nuñez, M. Chaparro, and J. Vilas (2002), Paleosecular variations 0–19,000 years recorded by sediments from Escondido Lake (Argentina), *Phys. Earth Planet. Inter.*, *133*, 35–55.

Gogorza, C., J. Lirio, H. Nuñez, M. Chaparro, H. Bertorello, and A. Sinito (2004), Paleointensity studies on Holocene–Pleistocene sediments from Lake Escondido, Argentina, *Phys. Earth Planet. Inter.*, *145*, 219–238.

Gogorza, C., M. Irurzun, M. Chaparro, J. Lirio, H. Nuñez, P. Bercoff, and A. Sinito (2006), Relative paleointensity of the geomagnetic field over the last 21,000 years BP from sediment cores, Lake El Trébol (Patagonia, Argentina), *Earth Planets Space*, *58*, 1323–1332.

Green, P., and B. Silverman (1994), *Nonparametric Regression and Generalized Linear Models: A Roughness Penalty Approach*, *Monogr. Stat. Appl. Probab.*, vol. 58, edited by D. R. Cox et al., CRC Press, London.

Gubbins, D. (2004), *Time Series Analysis and Inverse Theory for Geophysicists*, Cambridge Univ. Press, Cambridge, U. K.

Haltia-Hovi, E., N. Nowaczyk, and T. Saarinen (2010), Holocene palaeomagnetic secular variation recorded in multiple lake sediment cores from eastern Finland, *Geophys. J. Int.*, *180*, 609–622.

Hayashida, A., M. Ali, Y. Kuniko, H. Kitagawa, M. Torii, and K. Takemura (2007), Environmental magnetic record and paleosecular variation data for the last 40 kyrs from the Lake Biwa sediments, central Japan, *Earth Planets Space*, *59*, 807–814.

Hillenbrand, C.-D., J. A. Smith, G. Kuhn, O. Esper, R. Gersonde, R. D. Larter, B. Maher, S. G. Moreton, T. M. Shimmield, and M. Korte (2010), Age assignment of a diatomaceous ooze deposited in the western Amundsen Sea Embayment after the Last Glacial Maximum, *J. Quat. Sci.*, *25*, 280–295.

Hogg, E. (1978), The Holocene geomagnetic field in Europe, Ph.D. thesis, Univ. of Edinburgh, Edinburgh, U. K.

Huttunen, P., and J. Stober (1980), Dating of palaeomagnetic records from Finnish lake sediment cores using pollen analysis, *Boreas*, *9*, 193–202.

Hyodo, M. (1984), Possibility of reconstruction of the past geomagnetic field from homogeneous sediments, *J. Geomagn. Geoelectr.*, *36*, 45–62.

Hyodo, M., A. Yoshihara, K. Kashiwaya, T. Okimura, T. Masuzawa, R. Nomura, S. Tanaka, T. B. Xing, L. S. Qing, and L. S. Jian (1999), A Late Holocene geomagnetic secular variation record from Erhai Lake, southwest China, *Geophys. J. Int.*, *136*, 784–790.

Irurzun, M., C. Gogorza, M. Chaparro, J. Lirio, H. Nuñez, J. Vilas, and A. Sinito (2006), Paleosecular variations recorded by Holocene-Pleistocene sediments from Lake El Trébol (Patagonia, Argentina), *Phys. Earth Planet. Inter.*, *154*, 1–17.

Irving, E., and A. Major (1964), Post-depositional detrital remanent magnetization in a synthetic sediment, *Sedimentology*, *3*, 135–143.

Jackson, A., A. Jonkers, and M. Walker (2000), Four centuries of geomagnetic secular variation from historical records, *Philos. Trans. R. Soc. London A*, *358*, 957–990.

Johnson, E., T. Murphy, and O. Torreson (1948), Pre-history of the Earth's magnetic field, *Terr. Magn. Atmos. Electr.*, *53*, 349–372.

King, J. (1983), Geomagnetic secular variation curves for northeastern North America for the last 9000 years BP, Ph.D. thesis, Univ. of Minn., Minneapolis.

King, J., S. Banerjee, and J. Marvin (1983), A new rock-magnetic approach to selecting sediments for geomagnetic paleointensity studies: Application to paleointensity for the last 4000 years, *J. Geophys. Res.*, *88*, 5911–5921.

King, R. (1955), The remanent magnetism of artificially deposited sediments, *Mon. Not. R. Astron. Soc.*, *7*, 115–134.

Korte, M., and C. Constable (2003), Continuous global geomagnetic field models for the past 3000 years, *Phys. Earth Planet. Inter.*, *140*, 73–89.

Korte, M., and C. Constable (2005), Continuous geomagnetic field models for the past 7 millennia: 2. CALS7K, *Geochem. Geophys. Geosyst.*, *6*, Q02H16, doi:10.1029/2004GC000801.

Korte, M., and C. Constable (2006), On the use of calibrated relative paleointensity records to improve millennial-scale geomagnetic field models, *Geochem. Geophys. Geosyst.*, *7*, Q09004, doi:10.1029/2006GC001368.

Korte, M., and C. Constable (2008), Spatial and temporal resolution of millennial scale geomagnetic field models, *Adv. Space Res.*, *41*, 57–69, doi:10.1016/j.asr.2007.03.094.

Korte, M., and C. Constable (2011), Improving geomagnetic field reconstructions for 0–3 ka, *Phys. Earth Planet. Inter.*, *188*, 247–259.

Korte, M., A. Genevey, C. Constable, U. Frank, and E. Schnepp (2005), Continuous geomagnetic field models for the past 7 millennia: 1. A new global data compilation, *Geochem. Geophys. Geosyst.*, *6*, Q02H15, doi:10.1029/2004GC000800.

Korte, M., F. Donadini, and C. Constable (2009), Geomagnetic field for 0–3 ka: 2. A new series of time-varying global models, *Geochem. Geophys. Geosyst.*, *10*, Q06008, doi:10.1029/2008GC002297.

Korte, M., C. Constable, F. Donadini, and R. Holme (2011), Reconstructing the Holocene geomagnetic field, *Earth Planet. Sci. Lett.*, *312*, 497–505.

Lisé-Pronovost, A., G. St-Onge, S. Brachfeld, F. Barletta, and D. Darby (2009), Paleomagnetic constrains on the Holocene stratigraphy of the Arctic Alaskan margin, *Global Planet. Change*, *68*, 85–99.

Lund, S., and S. Banerjee (1985), Late Quaternary paleomagnetic field secular variation from two Minnesota lakes, *J. Geophys. Res.*, *90*, 803–825.

Lund, S., and L. Keigwin (1994), Measurement of the degree of smoothing in sediment paleomagnetic secular variation records: An example from Late Quaternary deep-sea sediments of the Bermuda Rise, western North Atlantic ocean, *Earth Planet. Sci. Lett.*, *122*, 317–330.

Menke, W. (1989), *Geophysical Data Analysis: Discrete Inverse Theory*, Acadamic, San Diego, Calif.

Mothersill, J. (1979), The paleomagnetic record of the late Quaternary sediments of Thunder Bay, *Can. J. Earth Sci.*, *16*, 1016–1023.
Mothersill, J. (1981), Late Quaternary record of the Goderich Basin, Lake Huron, *Can. J. Earth Sci.*, *18*, 448–456.
Mothersill, J. (1996), Paleomagnetic results from lakes Victoria and Albert, Uganda, *Stud. Geophys. Geod.*, *40*, 25–35.
Nilsson, A., I. Snowball, R. Muscheler, and C. B. Uvo (2010), Holocene geocentric dipole tilt model constrained by sedimentary paleomagnetic data, *Geochem. Geophys. Geosyst.*, *11*, Q08018, doi:10.1029/2010GC003118.
Nourgaliev, D., A. Borisov, F. Heller, B. Burov, P. Jasonov, D. Khasanov, and S. Ibragimov (1996), Geomagnetic secular variation through the last 3500 years as recorded by Lake Aslikul sediments from eastern Europe (Russia), *Geophys. Res. Lett.*, *23*, 375–378.
Nourgaliev, D., F. Heller, A. Borisov, I. Hajdas, G. Bonani, P. Iassonov, and H. Oberhänsli (2003), Very high resolution paleosecular variation record for the last ~1200 years from the Aral Sea, *Geophys. Res. Lett.*, *30*(17), 1914, doi:10.1029/2003GL018145.
Nourgaliev, D., F. Heller, A. Borisov, P. Yasonov, I. Chernova, and I. Hajdas (2005), Principal features (master curve) of geomagnetic field variations in Belorussia during the last 12 thousand years, *Russ. J. Earth Sci.*, *7*, 91–106.
Ojala, A., and T. Saarinen (2002), Palaeosecular variation of the Earth's magnetic field during the last 10,000 years based on the annually laminated sediment of Lake Nautäjarvi, central Finland, *Holocene*, *12*, 391–400, doi:10.1191/0959683602hl551rp.
Ojala, A., and M. Tiljander (2003), Testing the fidelity of sediment chronology: Comparison of varve and paleomagnetic results from Holocene lake sediments from central Finland, *Quat. Sci. Rev.*, *22*, 1787–1803.
Oldfield, F., P. R. J. Crooks, D. D. Harkness, and G. Petterson (1997), AMS radiocarbon dating of organic fractions from varved lake sediments: An empirical test of reliability, *J. Paleolimnol.*, *18*, 87–91.
Parker, R. (1994), *Geophysical Inverse Theory*, Princeton Univ. Press, Princeton, N. J.
Pavón-Carrasco, F., M. Osete, and J. Torta (2010), Regional modeling of the geomagnetic field in Europe from 6000 to 1000 B.C., *Geochem. Geophys. Geosyst.*, *11*, Q11008, doi:10.1029/2010GC003197.
Peck, J., J. King, S. Colman, and V. Kravchinsky (1996), An 84-kyr paleomagnetic record from the sediments of Lake Bailkal, Siberia, *J. Geophys. Res.*, *101*, 11,365–11,385.
Peng, L., and J. King (1992), A late Quaternary geomagnetic secular variation record from Lake Waiau, Hawaii, and the question of the Pacific nondipole low, *J. Geophys. Res.*, *97*, 4407–4424.
Rice, J. A. (1995), *Mathematical Statistics and Data Analysis*, Duxbury, Belmont, Calif.
Richter, C., A. Venuti, K. Verosub, and K.-Y. Wei (2006), Variations of the geomagnetic field during the Holocene: Relative palaeointensity and inclination record from the West Pacific (ODP Hole 1202B), *Phys. Earth Planet. Inter.*, *156*, 179–193.
Roberts, A., and M. Winklhofer (2004), Why are geomagnetic excursions not always recorded in sediments? Constraints from post-depositional remanent magnetization lock-in modelling, *Earth Planet. Sci. Lett.*, *227*, 345–359.
Saarinen, T. (1998), High-resolution palaeosecular variation in northern Europe during the last 3200 years, *Phys. Earth Planet. Inter.*, *106*, 299–309.
Schlossmacher, E. (1973), An iterative technique for absolute deviations curve fitting, *J. Am. Stat. Assoc.*, *68*, 857–859.
Snowball, I., and P. Sandgren (2002), Geomagnetic field variations in northern Sweden during the Holocene quantified from varved lake sediments and their implications for cosmogenic nuclide production rates, *Holocene*, *12*(5), 517–530, doi:10.1191/0959683602hl562rp.
Snowball, I., and P. Sandgren (2004), Geomagnetic field intensity changes in Sweden between 9000 and 450 cal BP: Extending the record of "archaeomagnetic jerks" by means of lake sediments and the pseudo-Thellier technique, *Earth Planet. Sci. Lett.*, *227*, 361–376, doi:10.1016/j.epsl.2004.09.017.
Snowball, I., L. Zillén, A. Ojala, T. Saarinen, and P. Sandgren (2007), FENNOSTACK and FENNORPIS: Varve dated Holocene palaeomagnetic secular variation and relative palaeointensity stacks for Fennoscandia, *Earth Planet. Sci. Lett.*, *255*, 106–116, doi:10.1016/j.epsl.2006.12.009.
Stanton, T., I. Snowball, L. Zillén, and S. Wastegård (2010), Validating a Swedish varve chronology using radiocarbon, palaeomagnetic secular variation, lead pollution history and statistical correlation, *Quat. Geochron.*, *5*, 611–624.
Stockhausen, H. (1998), Geomagnetic paleosecular variation (0–13,000 yr BP) as recorded in sediments from the three maar lakes from the West Eifel (Germany), *Geophys. J. Int.*, *135*, 898–910.
Stoner, J., A. Jennings, G. Kristjánsdóttir, G. Dunhill, J. Andrews, and J. Hardardóttir (2007), A paleomagnetic approach toward refining Holocene radiocarbon-based chronologies: Paleoceanographic records from the north Iceland (MD99-2269) and east Greenland (MD99-2322) margins, *Paleoceanography*, *22*, PA1209, doi:10.1029/2006PA001285.
St-Onge, G., J. Stoner, and C. Hillaire-Marcel (2003), Holocene paleomagnetic records from the St. Lawrence Estuary, eastern Canada: Centennial- to millennial-scale geomagnetic modulation of cosmogenic isotopes, *Earth Planet. Sci. Lett.*, *209*, 113–130.
St-Onge, G., T. M. D. Piper, C. Hillaire-Marcel, and J. Stoner (2004), Earthquake and flood-induced turbidites in the Saguenay Fjord (Québec): A Holocene paleoseismicity record, *Quat. Sci. Rev.*, *23*, 283–294.
Stuiver, M., and P. J. Reimer (1993), Extended ^{14}C data base and revised CALIB 3.0 ^{14}C age calibration program, *Radiocarbon*, *35*, 215–230.
Stuiver, M., P. J. Reimer, and T. F. Braziunas (1998), High-precision radiocarbon age calibration for terrestrial and marine samples, *Radiocarbon*, *40*, 1127–1151.
Suganuma, Y., J. Okuno, D. Heslop, A. Roberts, T. Yamazaki, and Y. Yokoyama (2011), Post-depositional remanent magnetization lock-in for marine sediments deduced from ^{10}Be and paleomagnetic records through the Matuyama-Brunhes boundary, *Earth Planet. Sci. Lett.*, *311*, 39–52, doi:10.1016/j.epsl.2011.08.038.
Tarantola, A. (2005), *Inverse Problem Theory and Methods for Model Parameter Estimation*, Soc. for Ind. Appl. Math., Philadelphia, Pa.
Tauxe, L. (1993), Sedimentary records of relative paleointensity of the geomagnetic field: Theory and practice, *Rev. Geophys.*, *31*, 319–354.
Tauxe, L. (2005), Inclination flattening and the geocentric axial dipole hypothesis, *Earth Planet. Sci. Lett.*, *233*, 247–261.
Tauxe, L., K. Kodama, and D. Kent (2008), Testing corrections for paleomagnetic inclination error in sedimentary rocks: A comparative approach, *Phys. Earth Planet. Inter.*, *169*, 152–165.
Thompson, R., and G. Turner (1985), Icelandic Holocene palaeolimnomagnetism, *Phys. Earth Planet. Inter.*, *38*, 250–261.
Thouveny, N., and D. Williamson (1988), Palaeomagnetic study of the Holocene and Upper Pleistocene sediments from Lake Barombi Mbo, Cameroun: First results, *Phys. Earth Planet. Inter.*, *52*, 193–206.
Turner, G. (1987), A 5000 year geomagnetic palaeosecular variation record from western Canada, *Geophys. J. R. Astron. Soc.*, *91*, 103–121.
Turner, G., and D. Lillis (1994), A palaeomagnetic secular variation record for New Zealand during the past 2500 years, *Phys. Earth Planet. Inter.*, *83*, 265–282.
Turner, G., and R. Thompson (1979), Behaviour of the Earth's magnetic field as recorded in the sediment of Loch Lomond, *Earth Planet. Sci. Lett.*, *42*, 412–426.
Turner, G., and R. Thompson (1981), Lake sediment record of the geomagnetic secular variation in Britain during Holocene times, *Geophys. J. R. Astron. Soc.*, *65*, 703–725.
Verosub, K., P. Mehringer, and P. Waterstraat (1986), Holocene secular variation in western North America: Paleomagnetic record from Fish Lake, Harney County, Oregon, *J. Geophys. Res.*, *91*, 3609–3623.
Vigliotti, L. (2006), Secular variation record of the Earth's magnetic field in Italy during the Holocene: Constraints for the construction of a master curve, *Geophys. J. Int.*, *165*, 414–429, doi:10.1111/j.1365-246X.2005.02785.x.
Wahba, G. (1990), *Spline Models for Observational Data*, Soc. for Ind. Appl. Math., Philadelphia, Pa.
Walker, M., and A. Jackson (2000), Robust modelling of the Earth's magnetic field, *Geophys. J. Int.*, *143*, 799–808, doi:10.1046/j.1365-246X.2000.00274.x.
Yamazaki, T. (1984), Thickness of the lock-in zone of post-depositional remanent magnetization in deep-sea silicious clay, *Rock Magn. Paleogeophys.*, *11*, 85–90.
Yang, X., F. Heller, J. Yang, and Z. Su (2009), Paleosecular variations since ~9000 yr BP as recorded by sediments from maar lake Shuangchiling, Hainan, south China, *Earth Planet. Sci. Lett.*, *288*, 1–9.
Zhu, R., Z. Gu, B. Huang, Z. Jin, X. Wei, and C. Li (1994), Geomagnetic secular variations and climate changes since 15,000 a BP, Beijing region, *Sci. China, Ser. B.*, *37*, 984–990.
Zillén, L. (2003), Setting the Holocene clock using varved lake lediments in Sweden, Ph.D. thesis, Lund Univ., Lund, Sweden.

F. Donadini, C. C. Finlay, A. M. Hirt, and S. Panovska, Institute of Geophysics, ETH Zürich, Sonneggstrasse 5, CH-8092 Zürich, Switzerland. (sanja.panovska@erdw.ethz.ch)